How Well Do Global Climate Models Simulate the Variability of Atlantic Tropical Cyclones Associated with ENSO?

HUI WANG,* LINDSEY LONG,* ARUN KUMAR,+ WANQIU WANG,+ JAE-KYUNG E. SCHEMM,+ MING ZHAO,# GABRIEL A. VECCHI,# TIMOTHY E. LAROW,@ YOUNG-KWON LIM,& SIEGFRIED D. SCHUBERT,** DANIEL A. SHAEVITZ,++ SUZANA J. CAMARGO,## NAOMI HENDERSON,## DAEHYUN KIM,## JEFFREY A. JONAS,@@ AND KEVIN J. E. WALSH&&

* *NOAA/NWS/NCEP/Climate Prediction Center, College Park, and Innovim, Greenbelt, Maryland*
+ *NOAA/NWS/NCEP/Climate Prediction Center, College Park, Maryland*
# *NOAA/Geophysical Fluid Dynamics Laboratory, Princeton, New Jersey*
@ *Center for Ocean-Atmospheric Prediction Studies, Florida State University, Tallahassee, Florida*
& *Global Modeling and Assimilation Office, NASA Goddard Space Flight Center, and Goddard Earth Sciences Technology and Research, I.M. Systems Group, Greenbelt, Maryland*
** *Global Modeling and Assimilation Office, NASA Goddard Space Flight Center, Greenbelt, Maryland*
++ *Department of Applied Physics and Applied Mathematics, Columbia University, New York, New York*
Lamont-Doherty Earth Observatory, Columbia University, Palisades, New York
@@ *Center for Climate System Research, Columbia University, and NASA Goddard Institute for Space Studies, New York, New York*
&& *School of Earth Sciences, University of Melbourne, Parkville, Victoria, Australia*

(Manuscript received 11 October 2013, in final form 10 April 2014)

ABSTRACT

The variability of Atlantic tropical cyclones (TCs) associated with El Niño–Southern Oscillation (ENSO) in model simulations is assessed and compared with observations. The model experiments are 28-yr simulations forced with the observed sea surface temperature from 1982 to 2009. The simulations were coordinated by the U.S. Climate Variability and Predictability Research Program (CLIVAR) Hurricane Working Group and conducted with five global climate models (GCMs) with a total of 16 ensemble members. The model performance is evaluated based on both individual model ensemble means and multimodel ensemble mean. The latter has the highest anomaly correlation (0.86) for the interannual variability of TCs. Previous observational studies show a strong association between ENSO and Atlantic TC activity, as well as distinctions during eastern Pacific (EP) and central Pacific (CP) El Niño events. The analysis of track density and TC origin indicates that each model has different mean biases. Overall, the GCMs simulate the variability of Atlantic TCs well with weaker activity during EP El Niño and stronger activity during La Niña. For CP El Niño, there is a slight increase in the number of TCs as compared with EP El Niño. However, the spatial distribution of track density and TC origin is less consistent among the models. Particularly, there is no indication of increasing TC activity over the U.S. southeast coastal region during CP El Niño as in observations. The difference between the models and observations is likely due to the bias of the models in response to the shift of tropical heating associated with CP El Niño, as well as the model bias in the mean circulation.

1. Introduction

It is well known that El Niño–Southern Oscillation (ENSO) strongly influences the interannual variability of Atlantic tropical cyclones (TCs). El Niño (La Niña) tends to suppress (enhance) Atlantic seasonal TC activity (e.g., Gray 1984; Pielke and Landsea 1999; Landsea 2000; Bell and Chelliah 2006). Although other climate modes, such as the Atlantic meridional mode, the North Atlantic Oscillation, and the Madden–Julian oscillation, also modulate North Atlantic TC activity (e.g., Kossin et al. 2010), here our focus is solely on ENSO. The state of ENSO is

Corresponding author address: Dr. Hui Wang, NOAA/Climate Prediction Center, 5830 University Research Court, NCWCP, College Park, MD 20740.
E-mail: hui.wang@noaa.gov

DOI: 10.1175/JCLI-D-13-00625.1

one of the key climate factors considered by the National Oceanic and Atmospheric Administration (NOAA) for their Atlantic hurricane season outlooks (NOAA 2013).

Using observational data, Kim et al. (2009) found distinct differences in Atlantic TC activity associated with eastern Pacific (EP) El Niño and central Pacific (CP) El Niño. The EP El Niño is the conventional El Niño with the warmest sea surface temperature (SST) anomalies in the tropical eastern Pacific, whereas CP El Niño or El Niño Modoki (Ashok et al. 2007) is a nonconventional El Niño with the warmest SST anomalies in the tropical central Pacific. The zonal shift of the warm SST anomalies indicates a change in tropical heating and consequent changes in atmospheric response.

A composite analysis of TC track density anomaly in Kim et al. (2009, their Fig. 2) displays coherent weakening in TC activity over the Caribbean Sea, Gulf of Mexico, and U.S. Atlantic East Coast region during EP El Niño and strengthened TC activity over the same regions during La Niña. Surprisingly, the composite for CP El Niño is also opposite to that for EP El Niño over these regions and closely resembles the La Niña composite. The results suggest a higher chance of landfalling TCs along the Gulf Coast and U.S. East Coast during CP El Niño than during EP El Niño.

It is well recognized that global climate models (GCMs), even at a low resolution, are able to simulate the interannual response of North Atlantic TCs to ENSO (e.g., Camargo et al. 2005; Zhao et al. 2009). Given the distinctions in the Atlantic TC activity associated with different El Niño types revealed in observations (Kim et al. 2009), it will also be interesting to know whether state-of-the-art GCMs can reproduce the different response to the two types of El Niño. Such a capability by models in distinguishing the responses of Atlantic TCs to different ENSO patterns is also important to both dynamical (e.g., Schemm and Long 2009) and statistical–dynamical (e.g., Wang et al. 2009; Vecchi et al. 2011) hurricane seasonal prediction systems.

With a primary focus on climate modeling studies of TCs, the U.S. Climate Variability and Predictability Research Program (CLIVAR) launched a Hurricane Working Group (HWG) in 2011 (U.S. CLIVAR 2011). To improve understanding of the interannual variability and trends in TC activity, as well as projections of future TC activity under a warming climate, the HWG initiated a series of simulations with high-resolution atmospheric GCMs (K. J. E. Walsh et al. 2014, unpublished manuscript). One set of simulations is the interannual experiment, which is Atmospheric Model Intercomparison Project (AMIP)-type simulations with multiple GCMs forced with the same observed time-varying SST from 1982 to 2009. This set of simulations provides necessary data to characterize TC response to ENSO in climate models.

This study aims to evaluate the performance of relatively high-resolution GCMs in simulating the interannual variability of Atlantic TCs associated with ENSO. The assessment is based on the analysis of AMIP-type simulations with five GCMs and comparisons with observations. The analysis targets one of the HWG objectives involving improved understanding of interannual variability of TC activity. The following three scientific questions are to be addressed in this study. How is the overall performance of GCMs in simulating the variability of Atlantic TCs? What are the characteristics of Atlantic TCs associated with ENSO in the models? What are the possible explanations for the differences between the models and observations? The study is expected to provide insights into the basic characteristics of Atlantic TC activity associated with different types of ENSO in GCMs.

This paper is organized as follows. Section 2 provides a brief description of data, models, and analysis methods used. Section 3 characterizes the Atlantic TC activity associated with ENSO in observations. The performance of GCMs in simulating the variability of the Atlantic TCs is assessed in section 4. Some possible explanations for the differences between the models and observations are explored in section 5. Conclusions are given in section 6.

2. Data and models

The data used in this study consist of SST, Atlantic TC tracks, precipitation, 500-hPa relative humidity, and 200-, 500-, and 850-hPa winds over a 28-yr (1982–2009) period from both observations and simulations with five atmospheric GCMs. For observations, the SST data are taken from the Hadley Centre Sea Ice and Sea Surface Temperature (HadISST) dataset (Rayner et al. 2003) on a $1° \times 1°$ (latitude $\times$ longitude) grid. The 28-yr monthly mean SSTs were also prescribed as low boundary forcing for the GCMs. The Atlantic TC track data are from the National Hurricane Center second-generation Atlantic hurricane database (HURDAT2; Landsea and Franklin 2013). The precipitation data are from the Climate Prediction Center (CPC) Merged Analysis of Precipitation (CMAP) dataset (Xie and Arkin 1997). Both the relative humidity and horizontal winds are from the National Centers for Environmental Prediction–U.S. Department of Energy (NCEP–DOE) Reanalysis 2 (R2; Kanamitsu et al. 2002). The precipitation data, as well as the reanalysis data, are monthly means on a $2.5° \times 2.5°$ grid.

Vertical wind shear is defined as the difference between the 200- and 850-hPa zonal winds. The zonal-wind shear is highly correlated with the entire wind shear field over the tropical North Atlantic (correlation > 0.9) and

TABLE 1. List of five GCMs for the HWG interannual experiments, the number of ensemble members, model data grid, and references for TC tracking algorithms.

Model	Ensemble members	Model data grid points (zonal × meridional)	Tracking algorithm
FSU	3	384 × 192	LaRow et al. (2008)
GFDL	3	576 × 360	Zhao et al. (2009)
GISS	3	360 × 180	Camargo and Zebiak (2002)
GSFC	2	576 × 361	LaRow et al. (2008)
GFS	5	360 × 181	Camargo and Zebiak (2002)

also dominates the variability of the entire wind shear over this basin (not shown). Therefore, the results obtained using the zonal-wind shear are expected to be consistent with those using the entire wind shear field. Similar to Colbert and Soden (2012), a deep-layer steering flow is derived based on the horizontal wind fields **V** at 850, 500, and 200 hPa, defined as $0.25\mathbf{V}_{850\text{hPa}} + 0.5\mathbf{V}_{500\text{hPa}} + 0.25\mathbf{V}_{200\text{hPa}}$.

The five GCMs employed for the HWG interannual experiments (1982–2009) are the Florida State University (FSU) model (Cocke and LaRow 2000), the Geophysical Fluid Dynamics Laboratory (GFDL) model (Zhao et al. 2009), the National Aeronautics and Space Administration (NASA) Goddard Institute for Space Studies (GISS) model E2 (Schmidt et al. 2014), the NASA Goddard Space Flight Center (GSFC) Earth Observing System Model, version 5 (GEOS-5; Rienecker et al. 2008; Molod et al. 2012), and the NCEP Global Forecast System (GFS) model (Saha et al. 2014). More detailed descriptions of the models can be found in K. J. E. Walsh et al. (2014, unpublished manuscript).

Table 1 lists the number of ensemble runs and model data resolutions, which are also close to model resolutions, as well as the references for TC tracking algorithms for the five models. The ensemble members vary from two to five with a total of 16 realizations. Horizontal resolutions range from about 0.5° to 1°. The TC track data were provided by each modeling group with different tracking algorithms. The differences in these TC detection methods include not only different variables but also different thresholds used. For example, the criterion required in Zhao et al. (2009) for the warm-core structure of TCs is a local maximum temperature averaged between 300 and 500 hPa, which is at least 1°C warmer than the surrounding local mean and located within 2° from the center of TCs. The criterion for the warm core in Camargo and Zebiak (2002) is the local 300–850-hPa mean warm temperature anomaly exceeding one standard deviation, based on the temperature anomalies at 300, 500, 700, and 850 hPa.

The Atlantic TC activity is quantified by the annual total number of TCs, as well as the spatial distribution of track density and TC origin. For observations, both subtropical storms and nondeveloping tropical depressions are excluded from HURDAT2. For the track density, the extratropical stages are also excluded from the observations. Given the spatially discrete nature of TC tracks, the track density is derived as follows: (i) the number of TCs passing through each 5° × 5° box during an entire hurricane season is first counted for each grid point centered in the 5° × 5° box on a 1° × 1° grid resolution; and (ii) the TC counts are then averaged with the TC numbers in the 5° × 5° boxes for eight surrounding grid points with a weighting coefficient of 0.5 for the center grid point and 1/16 for each surrounding grid point. This procedure is the same as for Kim et al. (2009) to ensure a spatially smoothed distribution. The TC origin is defined as the first point in HURDAT2 when the system becomes a tropical depression or a tropical storm. For the models, it is the first point detected by the TC tracking methods. Composites of SST, precipitation, vertical wind shear, relative humidity, and deep tropospheric steering flow anomalies averaged over August–October (ASO), the peak of the Atlantic hurricane season, are examined for different ENSO categories. The statistical significance of the composite anomalies is estimated by the Monte Carlo technique (e.g., Wilks 1995). The analysis is performed for both observations and multimodel ensemble (MME) mean, as well as individual model ensemble means. The MME mean is obtained by averaging individual model ensemble means. In this way, each model is treated with an equal weight for the MME, regardless of the number of ensemble members.

3. Variability of Atlantic TCs associated with ENSO in observations

During the 28-yr period (1982–2009), there were five EP El Niño (1982, 1986, 1991, 1997, and 2006) and five CP El Niño (1987, 1994, 2002, 2004, and 2009) years identified based on the definition of McPhaden et al. (2011), and eight La Niña years (1983, 1984, 1988, 1995, 1998, 1999, 2005, and 2007). Figure 1 shows the composite of ASO seasonal mean SST anomalies for EP El Niño, CP El Niño, and La Niña, respectively. Compared to EP El Niño (Fig. 1a), the SST anomalies in CP El Niño (Fig. 1b) shift toward the west. This may lead to significant differences in tropical heating for the atmosphere between the two types of El Niño. The amplitude of the CP El Niño SST anomalies (~1 K) is also smaller than the EP El Niño (~1.5 K), but comparable to the La Niña (~1 K, Fig. 1c).

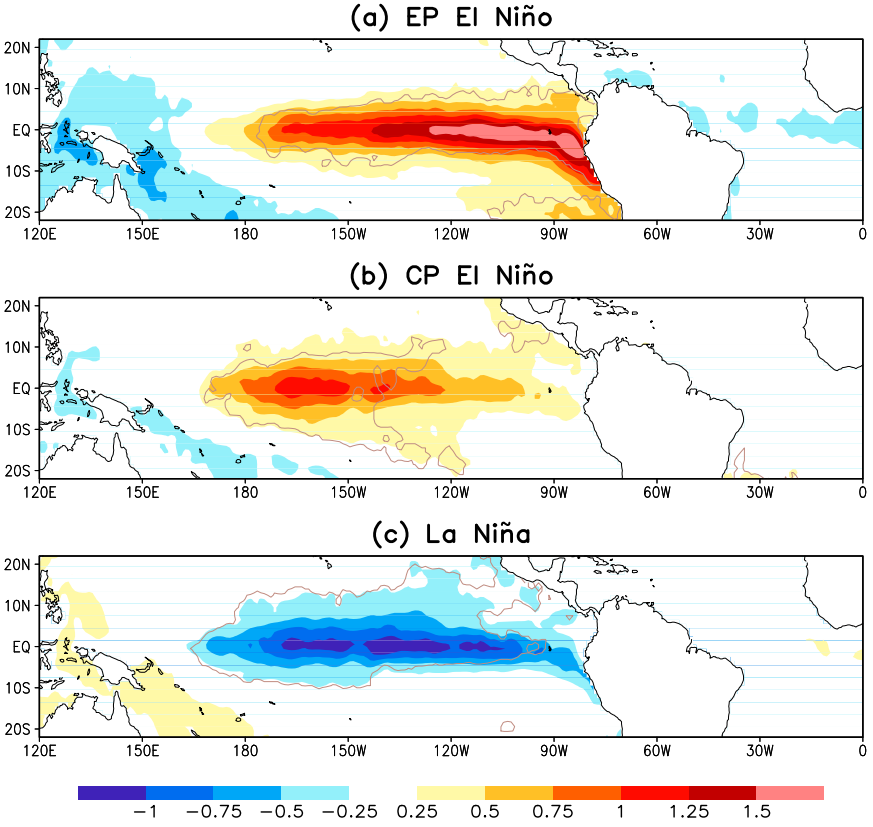

FIG. 1. Composites of ASO seasonal mean SST anomalies (K) for (a) EP El Niño (1982, 1986, 1991, 1997, and 2006), (b) CP El Niño (1987, 1994, 2002, 2004, and 2009), and (c) La Niña (1983, 1984, 1988, 1995, 1998, 1999, 2005, and 2007) during 1982–2009. The anomalies circled by light gray lines are above the 99% significance level estimated by the Monte Carlo test.

Similar composites are shown in Fig. 2 for TC track density (top row) and track density anomaly (middle row), respectively, associated with the three ENSO types. In La Niña years (Fig. 2c), track density displays high values (>1) across the North Atlantic basin. Areas with track densities greater than 1.5 are found in the central main development region (MDR; 10°–20°N, 20°–80°W), the Gulf of Mexico, and U.S. east coastal region. In contrast, track density is relatively low over these regions for EP El Niño (Fig. 2a), but increases considerably for CP El Niño (Fig. 2b), particularly in the MDR and U.S. southeast coastal region.

Consistent with the track density patterns, track density anomalies are generally below normal across the basin for EP El Niño (Fig. 2d), with the largest negative anomalies over the Gulf and MDR, and above normal during La Niña (Fig. 2f). Associated with CP El Niño (Fig. 2e), positive track density anomalies are found over the MDR, the Caribbean Sea, Gulf Coast and the southeastern coast, and negative anomalies farther to the east, as well as in the west Gulf of Mexico. The results indicate that relative to EP El Niño, there is a higher chance of landfalling TCs along the U.S. southeastern coast during CP El Niño.

The spatial distributions of total TC origins for the three ENSO categories are also shown in Fig. 2 (bottom). For a fair comparison with five EP El Niño and five CP El Niño, TC origins for La Niña are also shown for five episodes that occurred in the most recent years. There are increased TC origins over the MDR during CP El Niño (Fig. 2h) as compared to EP El Niño (Fig. 2g) and an additional increase of TC formation over the Gulf of Mexico during La Niña (Fig. 2i).

Although the sample size for ENSO composites is very limited over the 28 years, the composite anomalies in Fig. 2 (middle) are statistically significant above the 90% level. The anomaly patterns also resemble those in Kim et al. (2009) with longer records (57 yr, 1950–2006). Additionally, the sampling issue can be partially addressed by using HWG interannual experiments, which provide more atmospheric realizations than for the observations. Although the AMIP type of simulations does not increase the sample size of ENSO events, the ensemble of AMIP runs presented in the next section increases the sample size

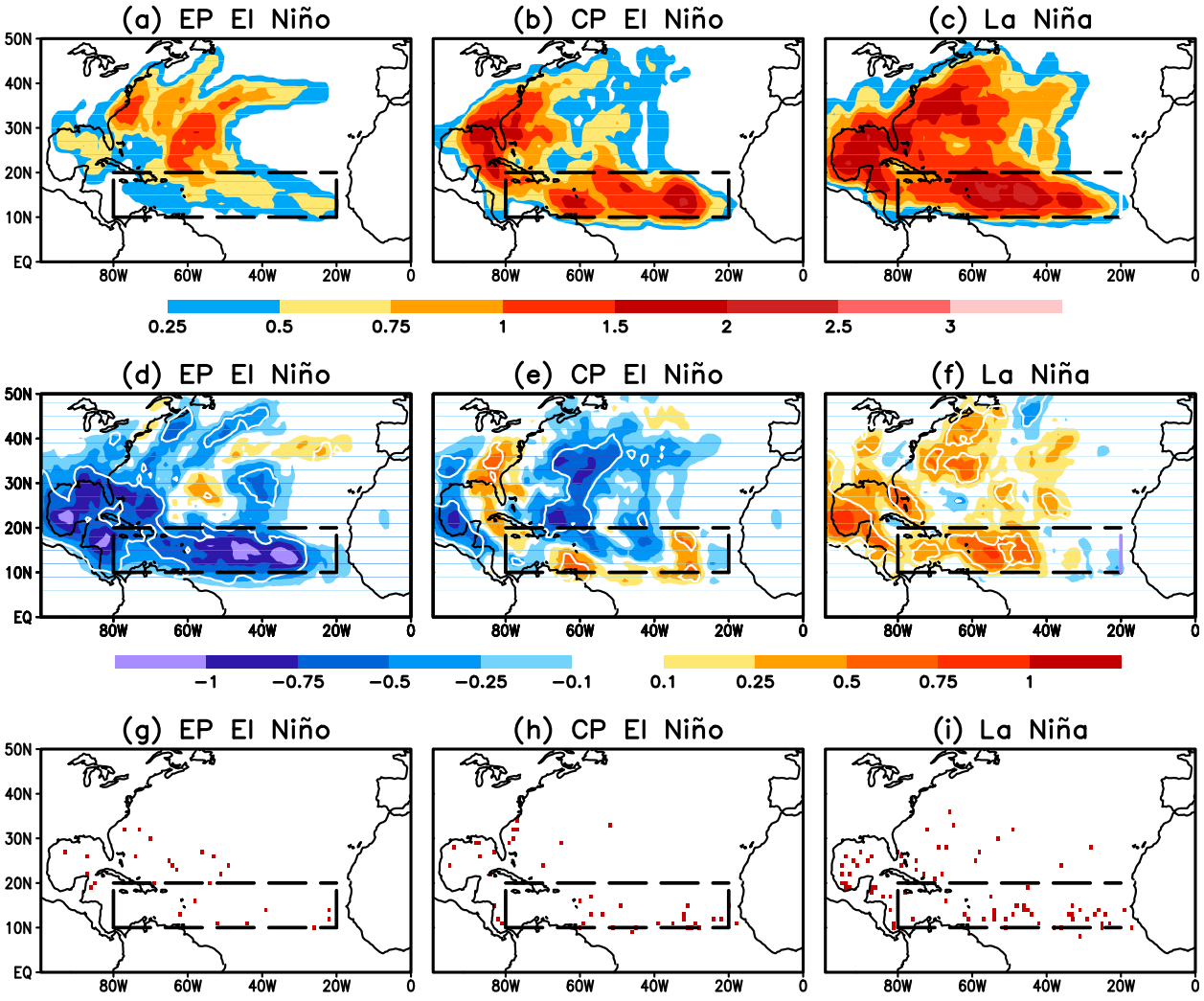

FIG. 2. Composites of (a)–(c) TC track density and (d)–(f) track density anomaly for (a),(d) EP El Niño, (b),(e) CP El Niño, and (c),(f) La Niña years, and distribution of TC origins during (g) five EP El Niño, (h) five CP El Niño, and (i) five La Niña years derived from observations. The anomalies circled by light white lines in (d)–(f) are above the 90% significance level estimated by the Monte Carlo test. The boxes with dashed lines denote the main development region (MDR; 10°–20°N, 20°–80°W).

of atmospheric realizations for a fixed set of ENSO events. This can effectively enhance the signal-to-noise ratio (Kumar and Hoerling 1995) and thereby provides a more reliable estimate for the ENSO-forced variability of the Atlantic TCs.

4. Variability of Atlantic TCs associated with ENSO in GCMs

The climatology and interannual variability of the annual number of Atlantic TCs are examined first. Figure 3a shows the time series of the annual number of Atlantic TCs from 1982 to 2009 for both observations and model simulations, including MME mean and individual model ensemble means. Both observations and MME display an upward trend over the 28-yr period. The gray shading in Fig. 3a denotes the range of ±1 standard deviation of the spreads of the five individual model ensemble means around the MME mean. Over 80% (23 out of 28 yr) of the observations fall into this range. Obviously, the GFS model has very high numbers of TCs and the GISS model has low numbers of TCs.

Table 2 summarizes the TC statistics for the observations and model simulations, including the climatological mean value, variance of interannual variability, linear trend over the 28 years, anomaly correlation (AC) between the models and observations (OBS), and root-mean-square error (RMSE). The GFDL model (12.7) and GSFC model (10.9) have a mean value close to the observations (11.7). In contrast, the climatology in the

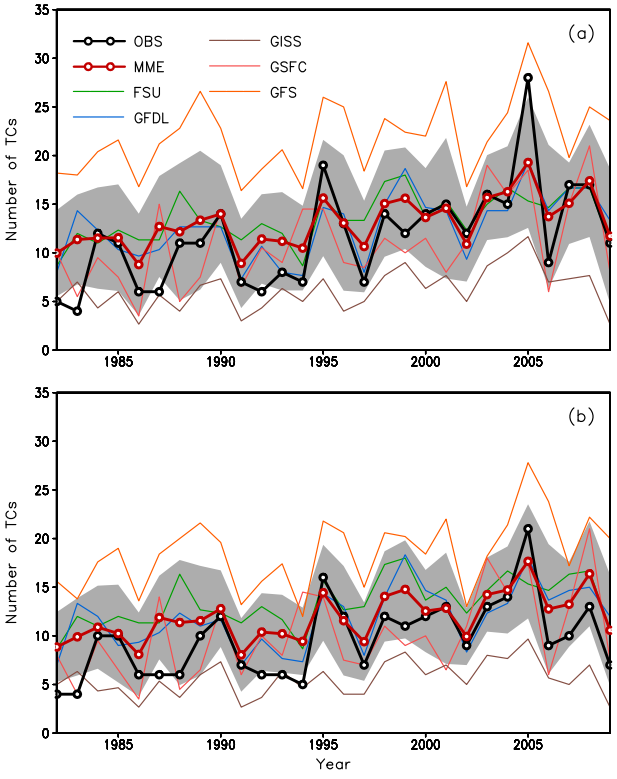

FIG. 3. (a) Time series of annual number of Atlantic TCs from 1982 to 2009 for observations (OBS) and multimodel ensemble (MME) mean (thick lines with open circles), as well as individual model ensemble means (thin lines). (b) Corresponding time series after short-lived TCs are removed. Gray shading denotes the range of ±1 std dev of the spreads of the five individual model ensemble means around the MME mean.

GISS model (6.2) is only about a half of the observations while the GFS model (22.0) has double the number in observations. The strength of the interannual variability in the GSFC and GFS models is comparable to observations and weaker in the other models and the MME. The linear trends in all models (~2 TCs decade^{-1}) are weaker than in the observations (~4 TCs decade^{-1}). AC is highest for the MME (0.86), followed by the GFDL (0.74) and GFS (0.73) models. This implies that 74% of the observed interannual TC variance is captured by the time series of the MME mean number of TCs and 54% is captured by the GFDL and GFS models. Additionally, the MME has the smallest RMSE. As a result of the large mean biases, the GFS and GISS models have relatively large RMSEs.

The correlation coefficients, such as 0.74 in the GFDL model, are close to that (0.78) in LaRow et al. (2008) based on the 20-yr TC rank correlation. However, this correlation for Atlantic TCs in the GFDL model (0.74) is less than the correlation (0.83) for Atlantic hurricanes in the same model (Zhao et al. 2009). The difference

TABLE 2. List of TC statistics for observations, MME mean, and individual model ensemble means, including 28-yr (1982–2009) long-term mean annual number of Atlantic TCs, variance of interannual variability, linear trend (increase of TCs per decade), anomaly correlation between observations and model-simulated interannual TC anomalies, and root-mean-square error. The variance for each model is the average of the variance derived from individual ensemble members. All the trends and ACs are above the 95% significance level.

Model	Mean	Variance	Trend	AC	RMSE
OBS	11.7	25.9	3.7		
MME	13.1	17.0	1.9	0.86	3.5
FSU	13.5	9.2	1.7	0.62	4.5
GFDL	12.7	16.4	2.2	0.74	3.6
GISS	6.2	8.8	1.1	0.68	6.7
GSFC	10.9	24.5	2.6	0.62	4.2
GFS	22.0	26.1	2.1	0.73	10.9

indicates that the model may have a better skill for intense TCs.

In terms of the five parameters in Table 2 (i.e., mean, interannual variability, trend, AC, and RMSE), the overall performance of the MME, GFDL, and GSFC models is better than that of the FSU, GISS, and GFS models. It should be noted that both the GFDL and GSFC models have a higher resolution than the other three models. This may suggest that a GCM with a higher resolution gets better performance in simulating the interannual variability of Atlantic TCs.

The observed trend showing an increase in the annual number of Atlantic TCs in HURDAT2 is much larger than the trend in the model simulations (Fig. 3a and Table 2). Landsea et al. (2010) found that the number of short-lived TCs (duration less than 2 days) in this dataset has increased markedly in the recent two decades. It is suggested that this variation is due to the changes in instrumentation and analysis methodology rather than changes in climate variability. Villarini et al. (2011) also confirmed that the long-term increase in the short-lived Atlantic TCs is closely associated with the changes in observing system over time. To assess how the short-lived TCs affect the results presented in Fig. 3a and Table 2, a similar analysis is performed with the annual number of TCs after the removal of the short-lived TCs from both the observations and model data, which are the TCs with winds of at least 18 m s^{-1} but lasting less than 2 days. The wind thresholds of 9 and 12 m s^{-1} are used for the Atlantic TCs in the GISS and GSFC models, respectively, because of relatively weak winds associated with the TCs in the two models.

The time series of the annual number of Atlantic TCs without the short-lived TCs are shown in Fig. 3b, and the corresponding TC statistics are summarized in Table 3.

TABLE 3. As in Table 2, but for corresponding TC statistics when short-lived TCs are removed from the annual number of TCs. Values in parentheses are the percentage changes of mean and variance due to the removal of the short-lived TCs.

Model	Mean	Variance	Trend	AC	RMSE
OBS	9.7 (17%)	15.0 (42%)	2.5		
MME	11.9 (9%)	15.5 (9%)	1.8	0.85	3.1
FSU	13.4 (1%)	9.4 (2%)	1.7	0.61	4.8
GFDL	11.8 (7%)	14.4 (12%)	1.9	0.70	3.5
GISS	5.6 (10%)	6.7 (24%)	0.8	0.68	5.0
GSFC	10.1 (7%)	23.7 (3%)	2.6	0.57	3.9
GFS	18.6 (15%)	23.4 (10%)	2.0	0.76	9.3

TABLE 4. Mean annual number of TCs over the entire 28 years, five EP El Niño, five CP El Niño, and eight La Niña years, respectively, for observations, MME, and individual model ensemble means. Values in parentheses are the percentages of the 28-yr climatology.

Model	Mean	EP El Niño	CP El Niño	La Niña
OBS	11.7	6.8 (58%)	10.2 (87%)	14.6 (125%)
MME	13.1	10.4 (80%)	12.4 (95%)	14.5 (111%)
FSU	13.5	11.9 (88%)	12.0 (89%)	15.3 (113%)
GFDL	12.7	9.5 (75%)	11.0 (87%)	15.5 (122%)
GISS	6.2	4.5 (73%)	5.7 (91%)	7.3 (117%)
GSFC	10.9	6.9 (63%)	12.9 (118%)	11.2 (102%)
GFS	22.0	19.3 (88%)	20.5 (93%)	23.1 (105%)

The removal of the short-lived TCs leads to a 17% reduction of the annual mean TC counts and a 42% reduction of TC variance in the observations (Table 3). The changes in the GCMs are small, ranging from 1% to 15% for the annual mean and from 2% to 24% for the variance. The trend in the annual TC frequency decreases by 1.2 TCs decade^{-1} in the observations and by 0.3 TC decade^{-1} or less in the models. As a result, the simulated trend is closer to the observations in Table 3 than in Table 2. Overall, there are no significant changes in AC between the two tables but a slight decrease of RMSE in Table 3. The results suggest that the short-lived TCs influence HURDAT2 more than the model data, consistent with the findings of Landsea et al. (2010) and Villarini et al. (2011). In the following analysis, the short-lived TCs are retained in both the model data and the observations.

The average number of TCs for each ENSO category is examined in Table 4 and compared with the corresponding 28-yr climatology for both observations and simulations. In the observations, there are about 7, 10, and 15 TCs each hurricane season in EP El Niño, CP El Niño, and La Niña years, respectively, equivalent to 58%, 87%, and 125% of the mean value (11.7). All models show consistent increases in the number of TCs from EP El Niño to CP El Niño and further increases to La Niña, except for the GSFC model. However, the changes in TC counts from one ENSO type to another in the models are much more conservative than in the observations. In the MME, for instance, there is a 15% increase in TCs from EP El Niño to CP El Niño and an additional 16% increase to La Niña in terms of the mean value. The corresponding changes in observations are 29% and 38%. The results indicate a weaker interannual variability of Atlantic TCs in the model simulations. It should also be noted that the MME mean approach, by averaging out random variability, may reduce the variability of TC counts in the models.

The spatial characteristics of mean TC activity are presented in Fig. 4 for both observations and simulations in the form of 28-yr mean track densities and total TC origins during the entire 28 years. Compared to the observations (Fig. 4a), each model has different mean biases. Among the five models, the GFDL model (Fig. 4d) is closest to the observations for both the magnitude and spatial coverage of track density. The FSU, GSFC, and GFS models (Figs. 4c,f,g) have a very high track density (>3) over the west MDR, east-central MDR, and most of the North Atlantic basin, respectively, whereas the GISS model (Fig. 4e) has a very low track density over the entire basin. The MME mean pattern (Fig. 4h) shows a higher track density in the MDR than the observations (Fig. 4a). The track density over the U.S. east coastal regions is close to the observations. Overall, the MME is better than most individual models.

The TC origins in observations (Fig. 4b) are characterized by two regions with large populations—one over the MDR and the other over the Gulf of Mexico—and adjacent sectors of the Atlantic Ocean and Caribbean Sea. The FSU, GSFC, and GFS models exhibit very dense TC origins over the central and to the south of the MDR (Fig. 4i), to the south of the east MDR (Fig. 4l), and to the south and east of the MDR (Fig. 4m), respectively. The GISS model shows a lack of TC formations over the east MDR. The GFDL model (Fig. 4j) and MME (Fig. 4n) have a distribution of TC origins closer to the observations than the other models. The model biases in the distribution of TC origins are consistent with the biases of track density and mean number of TCs. For example, the dense TC origins in the FSU and GSFC models (Figs. 4i,l) lead to high track density over the regions to the northwest of the TC origins (Figs. 4c,f).

Similar to the ENSO composites of track density for observations (Fig. 2, top), Fig. 5 displays the ENSO composites of track density for individual model ensemble means, as well as MME mean. In spite of the distinct biases in each model revealed in Fig. 4, the composites consistently show relatively low track densities during EP El Niño (Fig. 5, left) in all models and

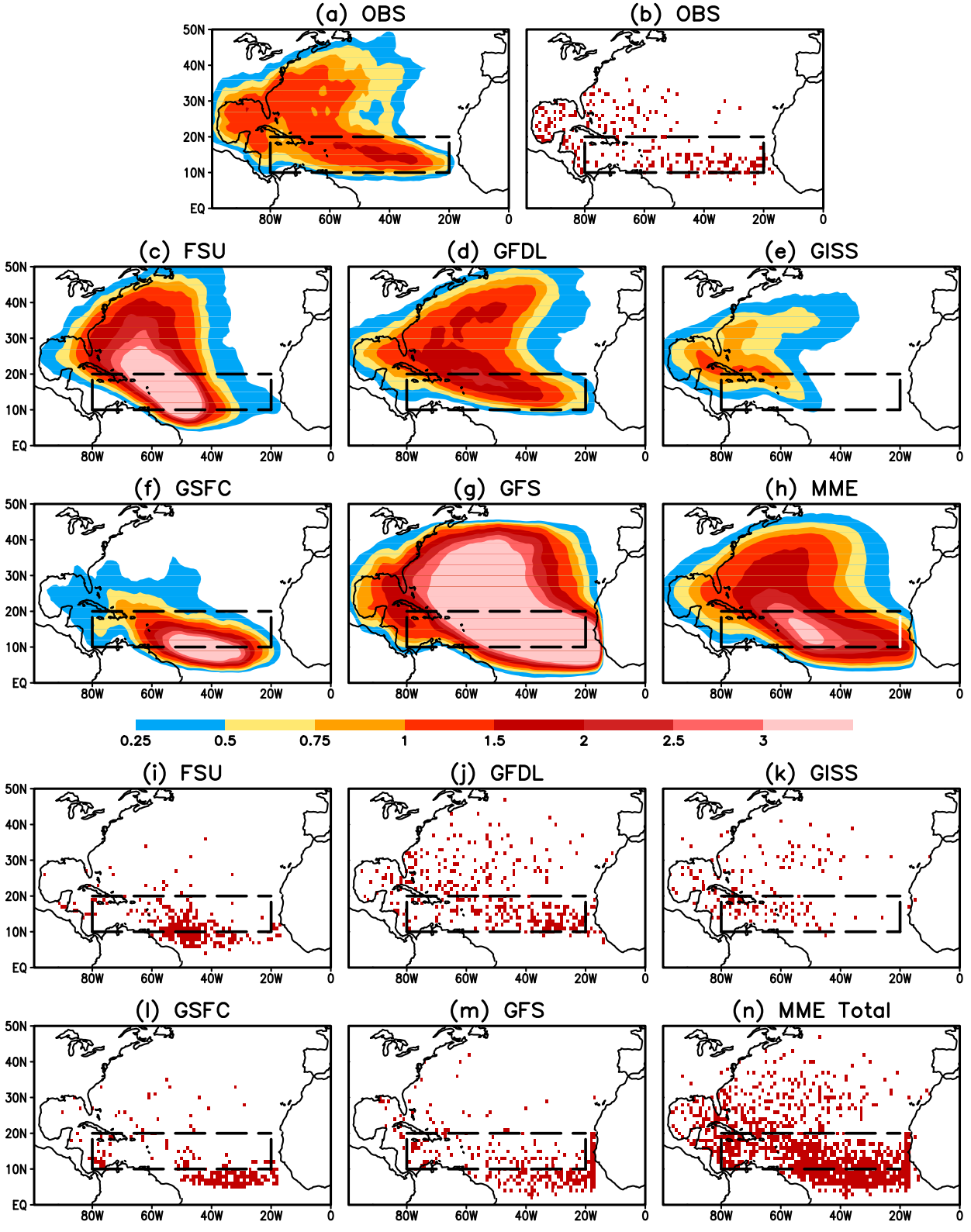

FIG. 4. Climatology of track density for (a) observations, (c)–(g) individual model ensemble means, and (h) MME mean, and 28-yr total TC origins for (b) observations, (i)–(m) one ensemble member of each model, and (n) MME total from one member of each model. The boxes with dashed lines denote the MDR.

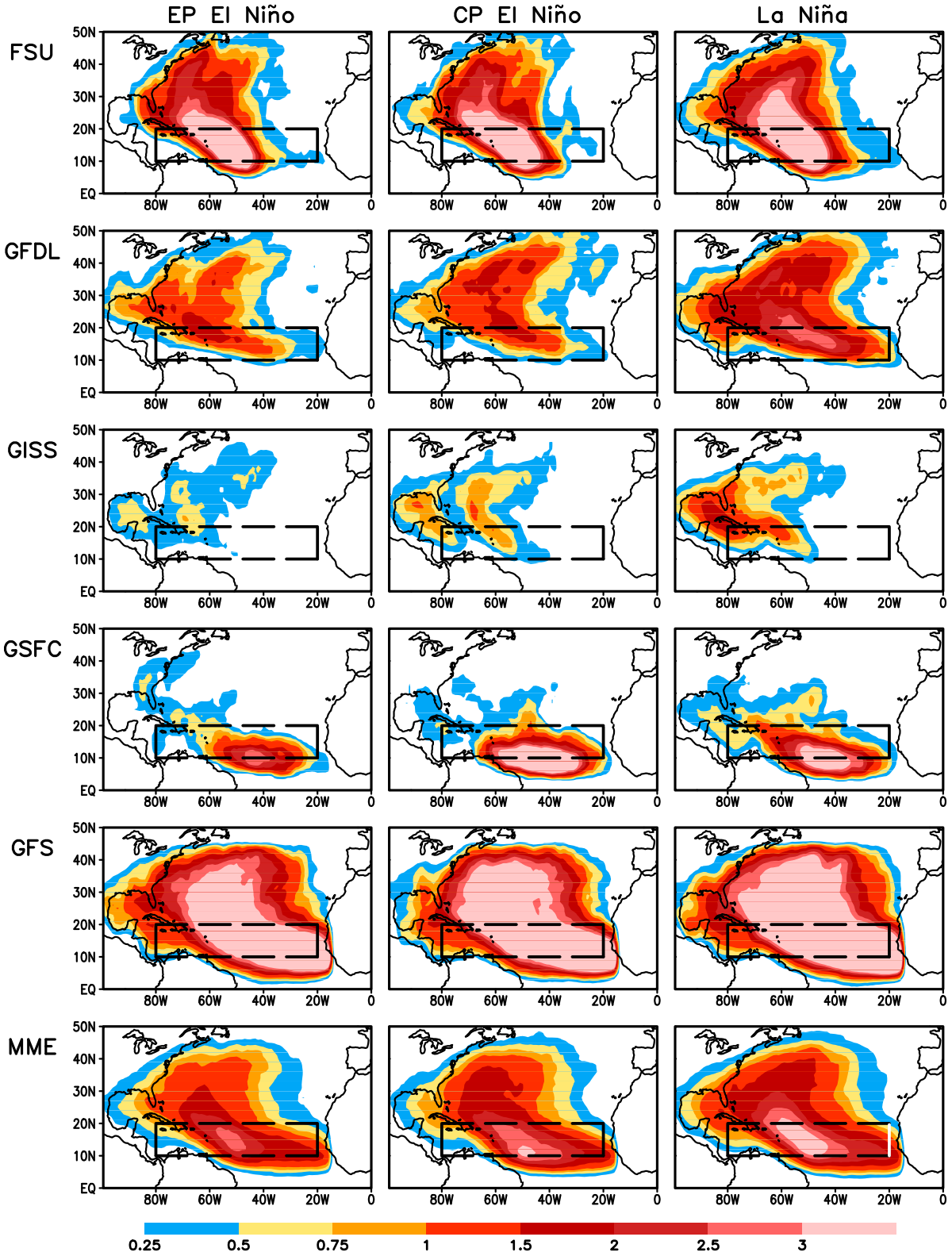

FIG. 5. Composites of track density during (left) EP El Niño, (center) CP El Niño, and (right) La Niña for five individual model ensemble mean and (bottom) MME mean. The boxes with dashed lines denote the MDR.

high track densities during La Niña in most models (Fig. 5, right), except for the GSFC model. Furthermore, there is a clear increase in track density from EP El Niño to CP El Niño (Fig. 5, center).

The corresponding composites for track density anomaly are illustrated in Fig. 6. The track density anomalies in the GCMs are generally below normal across the basin during EP El Niño (Fig. 6, left) and above normal during La Niña (Fig. 6, right). In some spots, the negative anomalies associated with EP El Niño (left column) become positive during CP El Niño (Fig. 6, center). The results in Figs. 5 and 6 suggest that the GCMs are able to capture some of the observed features of the Atlantic TC activity associated with ENSO. Qualitatively, there is less TC activity associated with EP El Niño, more activity associated with La Niña, and increasing TC activity during CP El Niño with respect to EP El Niño. However, the patterns of track density vary from model to model and differ from observations. Particularly, there are no indications of increasing landfalling TCs along the U.S. southeastern coast during CP El Niño in the model simulations.

The modeled TC origins over five years from one ensemble member of each model are shown in Fig. 7 for each ENSO category. Relative to EP El Niño (Fig. 7, left), there are increases in the formation of TCs over or near the MDR during CP El Niño (Fig. 7, center) and La Niña (Fig. 7, right) in some models, such as the GSFC and GFS models. Only the GFDL model shows some increase in TC origins at high latitudes between 20° and 40°N, especially during CP El Niño. Unlike observations (Fig. 2i), there are no increases in TC origins over the Gulf of Mexico and west Caribbean Sea in all models during La Niña. This may be related to the model bias in simulating the TC formations over these regions (Fig. 4). The differences in TC origins among the three ENSO categories in the MME (Fig. 7, bottom) are not as large as in the observations (Fig. 2, bottom). This is another indication of relatively weak interannual variability of Atlantic TCs in GCMs.

5. Possible explanations for model biases

The changes in both the mean and variability of Atlantic TCs is accompanied by changes in atmospheric circulation (e.g., Goldenberg and Shapiro 1996; Goldenberg et al. 2001). Therefore, in order to understand the mean biases of TC activity in GCMs, Fig. 8 shows the ASO season climatology of vertical shear of zonal wind between 200 and 850 hPa derived from observations and mean biases for individual model ensemble means and the MME mean. The regions of weak mean vertical wind shear ($<10\,\mathrm{m\,s^{-1}}$, Fig. 8a) coincide with the regions of high mean track density and TC origins in observations (Figs. 4a,b).

The mean bias in the vertical wind shear may account for the mean bias in Atlantic TC activity in some models. In the FSU model (Fig. 8b), for instance, a large negative bias of vertical wind shear (over $-10\,\mathrm{m\,s^{-1}}$) in the west MDR leads to a close-to-zero mean state of vertical wind shear, which favors the generation and development of TCs. This is consistent with the mean bias of high track density and TC origins over this region (Figs. 4c,i). In the GISS model (Fig. 8d), a positive bias of vertical wind shear in the east MDR enhances the mean vertical wind shear and prevents TCs from occurring over this area. As a result, TC tracks and TC origins shift toward the west (Figs. 4e,k).

Both individual model ensemble means (Figs. 8b–f) and the MME mean (Fig. 8g) exhibit negative biases in vertical wind shear over and/or near the MDR and positive biases to the north, especially over the Gulf Coast and U.S. southeastern coast. Consequently, there are biases of high track density and dense TC origins at low latitudes and low track density and sparse TC origins over the Gulf and U.S. southeastern coast in the models (Fig. 4). The negative wind shear biases over the MDR are mainly due to too weak upper-level westerlies in the models (not shown). The striped pattern of the vertical zonal-wind shear biases (Fig. 8) is likely related to improperly simulating the tropical upper-tropospheric trough (Fitzpatrick et al. 1995). More specifically, having a weaker upper-level trough in the models will alter the location of the trough relative to the trade winds, leading to lower wind shear over the MDR and higher wind shear over the subtropics.

Figure 9 displays the composites of ASO season vertical wind shear anomalies associated with the three ENSO categories for observations (Figs. 9a–c) and MME (Figs. 9d–f), respectively. Overall, the model circulation response to different ENSO SST anomalies agrees with the observations, both with positive vertical wind shear anomalies to the south of 20°N associated with EP El Niño (Fig. 9, left) and negative anomalies associated with La Niña (Fig. 9, right). The circulation response to CP El Niño is less significant or less spatially coherent over the subtropical North Atlantic (Fig. 9, center). This is likely due to the weak amplitude and small area coverage of the CP El Niño SST anomalies (Fig. 1). Thus, the atmospheric response may be weak (e.g., Wang et al. 2013). In spite of that, it is still evident that wind shear anomalies over the MDR are largely reduced as compared to EP El Niño, a condition that is more favorable for TC activity during CP El Niño. The results present in Fig. 9 are also consistent with the better simulations of Atlantic TC activity in GCMs for EP El Niño and La Niña than for CP El Niño.

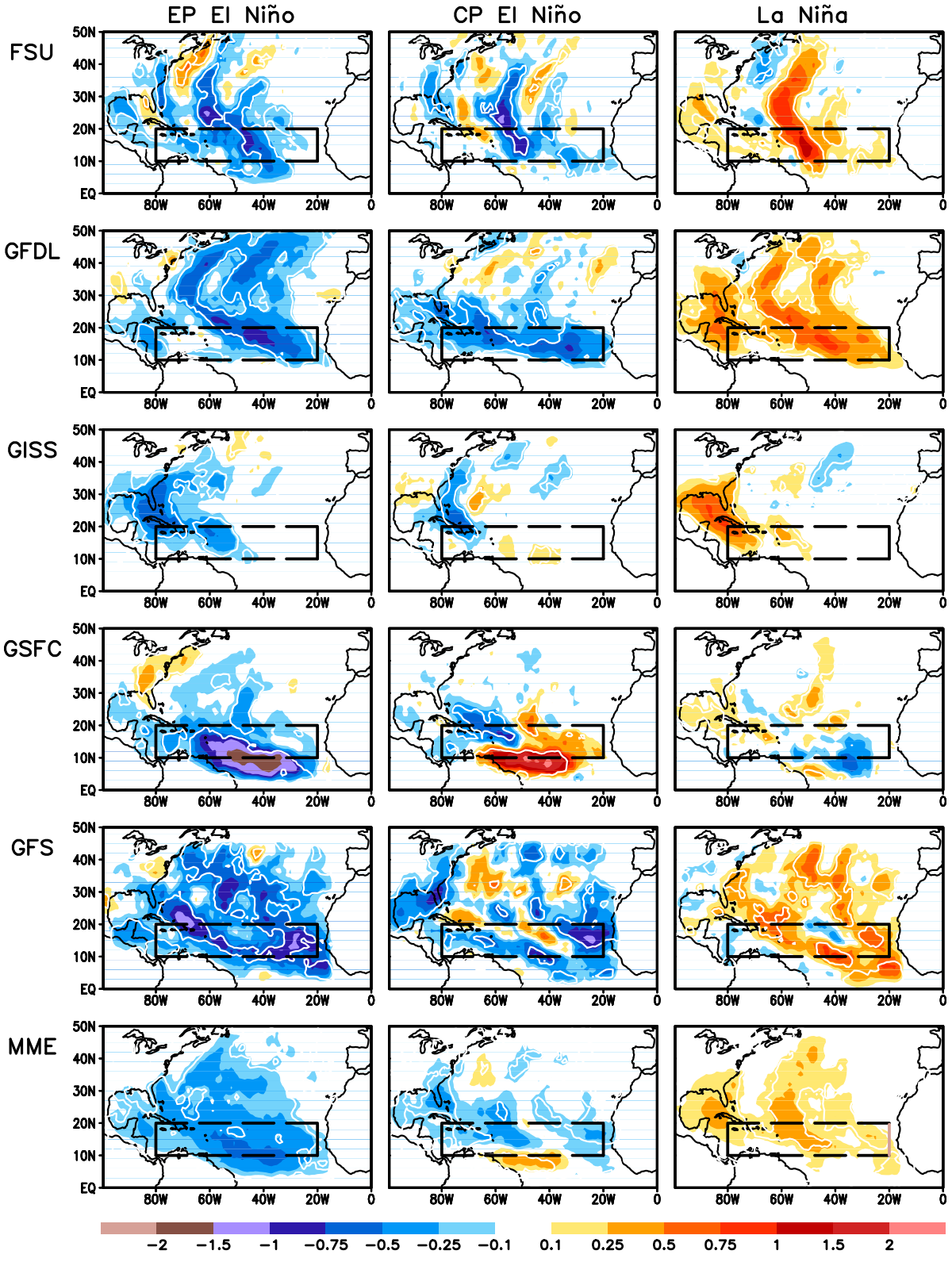

FIG. 6. Composites of track density anomaly during (left) EP El Niño, (center) CP El Niño, and (right) La Niña for five individual model ensemble mean and (bottom) MME mean. The anomalies circled by light white lines are above the 90% significance level. The boxes with dashed lines denote the MDR.

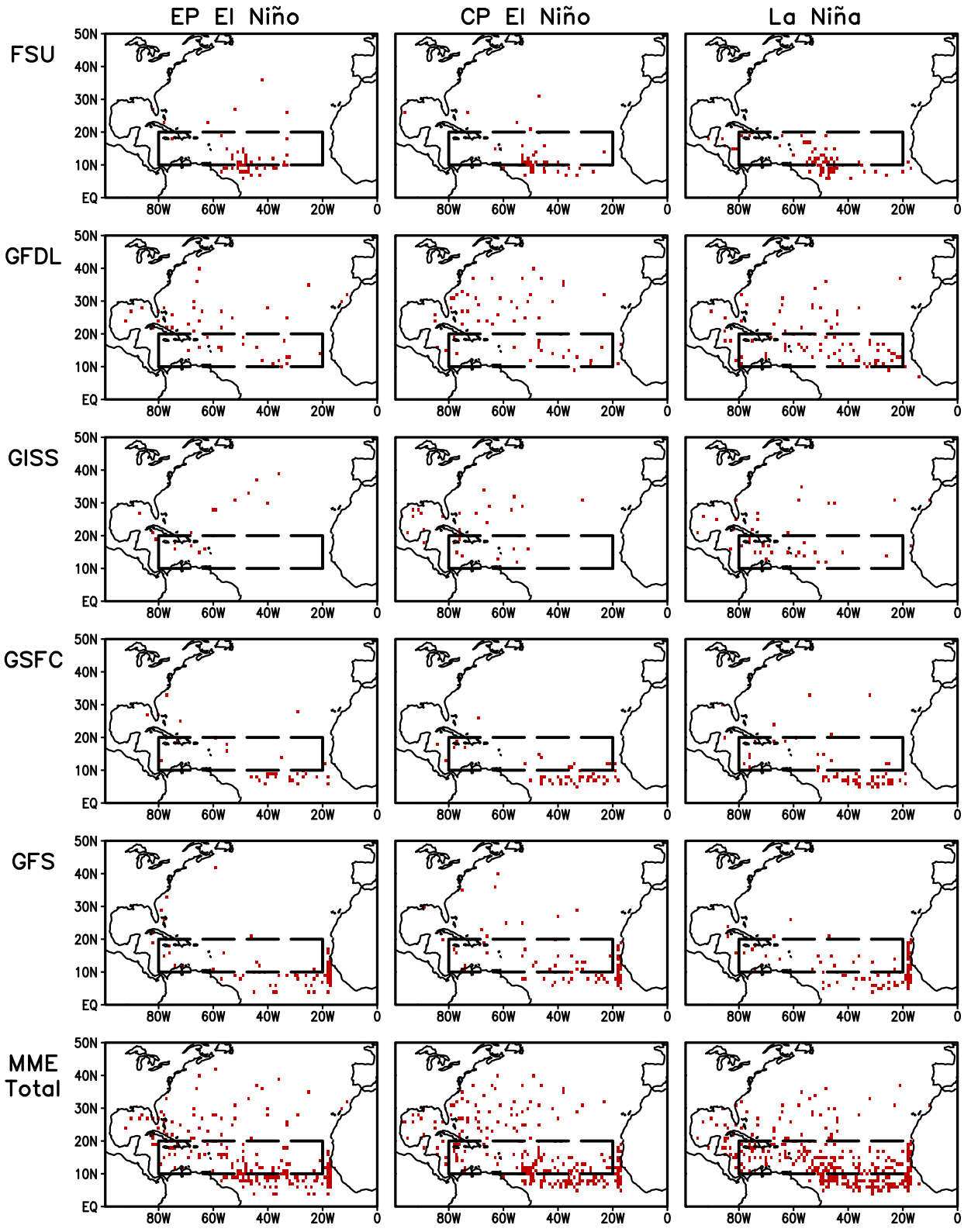

FIG. 7. Distribution of TC origins during five (left) EP El Niño, (center) five CP El Niño, and (right) five La Niña years from one ensemble member of each model and (bottom) MME total from one member of each model. The boxes with dashed lines denote the MDR.

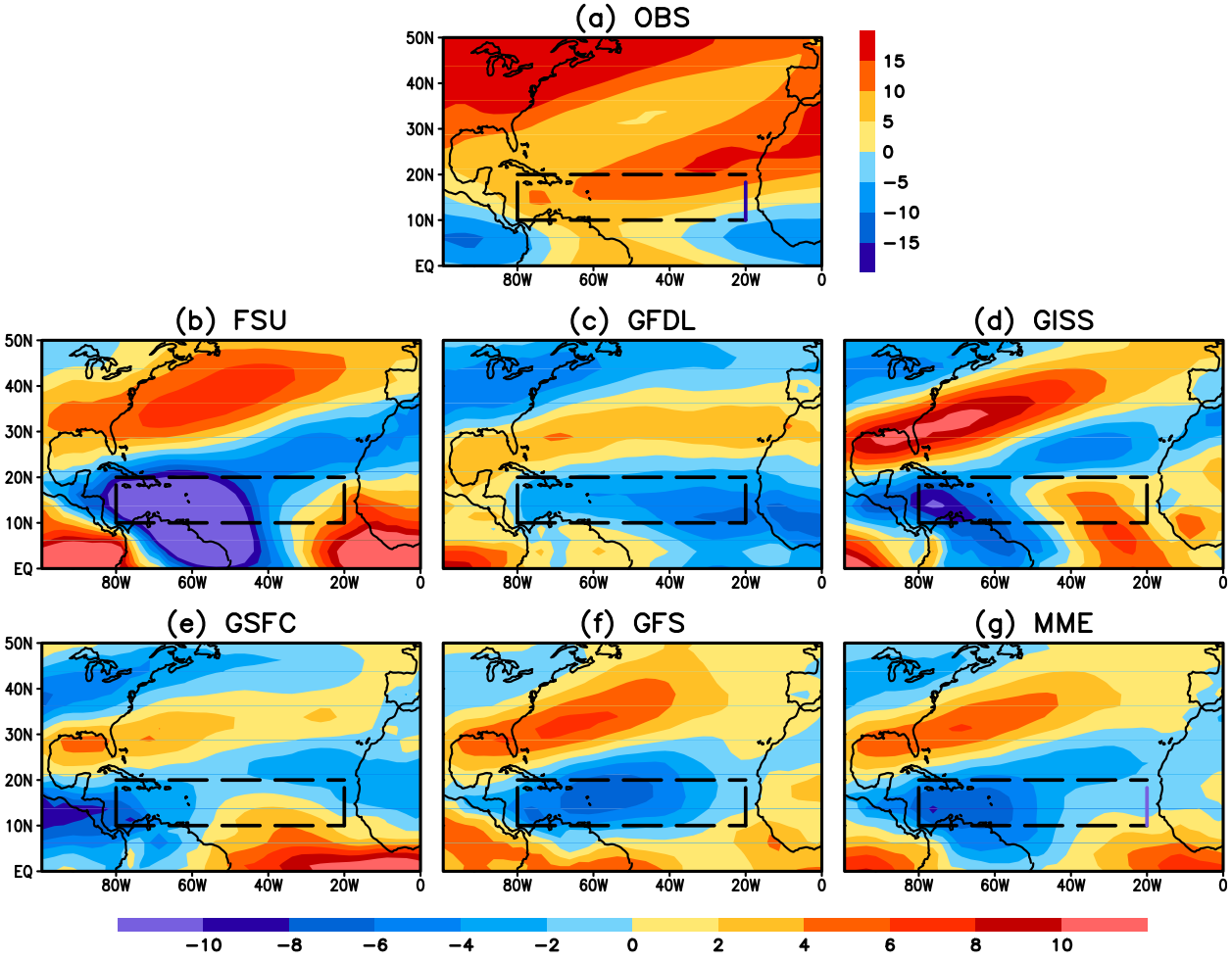

FIG. 8. (a) Observed ASO season climatology of vertical shear of zonal wind ($m\,s^{-1}$) between 200 and 850 hPa and mean bias in the (b) FSU, (c) GFDL, (d) GISS, (e) GSFC, and (f) GFS models, as well as (g) the MME. The boxes with dashed lines denote the MDR.

ENSO influences the Atlantic TC activity by altering vertical wind shear (e.g., Goldenberg and Shapiro 1996) and atmospheric stability (Tang and Neelin 2004) over the Atlantic through atmospheric teleconnection. It may also change tropical Atlantic SST via local air–sea interaction (Enfield and Mayer 1997), which in turn affects the TC activity (Goldenberg et al. 2001). The composites of SST anomalies in Fig. 1 suggest very weak Atlantic SST anomalies associated with ENSO in ASO. Furthermore, diagnostics of the ENSO modulation of TC activity using a genesis potential index identified vertical wind shear as one of the main environmental factors responsible for this modulation in the North Atlantic (Camargo et al. 2007). Therefore, the atmospheric response to tropical heating related to ENSO SST and atmospheric teleconnection are likely the primary processes responsible for the ENSO impact.

The westward shift of warm SST anomalies from EP El Niño to CP El Niño (Fig. 1) may lead to changes in tropical heating. In the tropics, precipitation associated with deep convection is a good indicator of tropical heating in the atmosphere. Similar to Wang et al. (2012), the composites of ASO season precipitation anomalies over the tropical Pacific are used to illustrate and verify the changes in tropical heating, as shown in Fig. 10. In both observations and the MME mean of the GCM simulations, associated with EP El Niño (Figs. 10a,d), there are positive precipitation anomalies across the central and eastern equatorial Pacific. Associated with CP El Niño (Figs. 10b,e), precipitation anomalies shift toward the west with no large anomalies over the eastern Pacific. In La Niña, negative precipitation anomalies cross the tropical Pacific (Figs. 10c,f). In general, the GCMs reproduce the observed major features of precipitation anomalies over the tropical Pacific for different types of ENSO. On the other hand, precipitation response to ENSO over the tropical North Atlantic varies considerably across the models (not shown), which

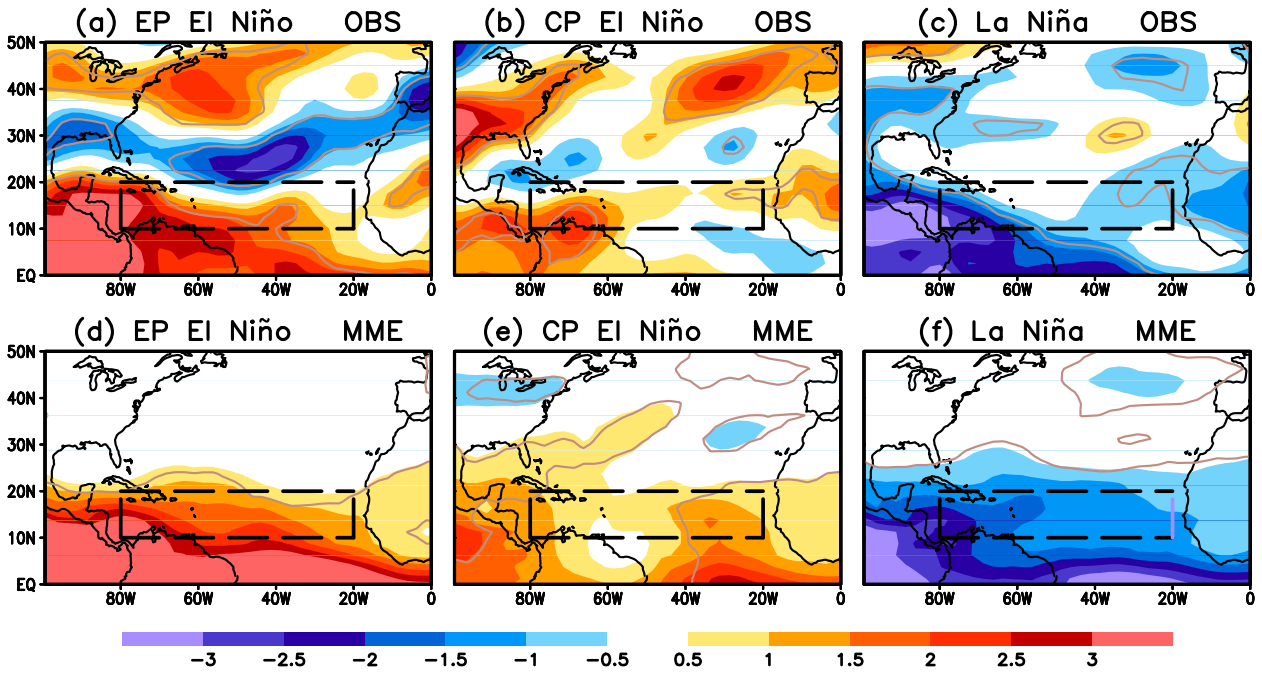

FIG. 9. Composites of ASO seasonal mean vertical wind shear anomalies ($m\,s^{-1}$) for (a),(d) EP El Niño; (b),(e) CP El Niño; and (c),(f) La Niña during 1982–2009 in (a)–(c) observations and (d)–(f) the MME mean. The anomalies circled by light gray lines are above the 90% significance level. The boxes with dashed lines denote the MDR.

may contribute to the model diversity in simulating the TC variability associated with ENSO.

There are also differences in precipitation between observations and simulations over the tropical Pacific, such as weaker precipitation anomalies in the models between 160°E and the date line for all ENSO categories. These differences may be related to model convection schemes and model sensitivity to SST. Together with model biases in mean circulation (not shown), they may modify the Rossby wave source (Sardeshmukh and Hoskins 1988) and thus affect the detailed structure of circulation response to ENSO.

Figure 11 gives a simple example of changes in vertical wind shear associated with a westward shift of warm SST anomalies from the Niño-3 region (5°S–5°N, 90°–150°W) to the Niño-4 region (5°S–5°N, 150°W–160°E). First, the ASO season vertical wind shear anomalies are regressed against the Niño-4 and Niño-3 SST indices, separately. The differences between the two sets of regression coefficients are shown for observations (Fig. 11a) and the MME (Fig. 11b), respectively. Both the observations and the MME exhibit a similar large-scale wave train pattern originating from the western and central equatorial Pacific and along a great circle route to tropical Atlantic. A closer inspection of Fig. 11 reveals some differences in the changes of vertical wind shear over the tropical North Atlantic between the observations and simulations. Negative wind shear anomalies are found to the north of the MDR in the observations (Fig. 11a) whereas positive anomalies are found over the MDR in the MME (Fig. 11b). The results illustrate the difference between the observations and GCMs in North Atlantic vertical wind shear response to the shift of tropical Pacific SST anomalies. The difference may cause further changes in the responses of Atlantic TCs to the shift of SST anomalies.

In addition to the vertical wind shear, the large-scale humidity field also affects both mean TC activity (Peng et al. 2012) and the ENSO-related variability (Camargo et al. 2007). Figure 12 shows the ASO season climatology of 500-hPa relative humidity over the tropical and North Atlantic for both observations and the MME mean, as well as the composite anomalies of 500-hPa relative humidity for the three ENSO categories. The ASO mean atmosphere is more moistened in the models than in the observations (Figs. 12a,b). The mean humidity field is thus more favorable for TC genesis and development (Peng et al. 2012) in the GCMs than in the observations, consistent with the higher mean track density in the MME (Figs. 4a,h).

Overall, the ENSO-related humidity variability over the North Atlantic basin is weaker in the models (Fig. 12, bottom) than in the observations (Fig. 12, middle). This is partially due to the MME averaging, as well as the

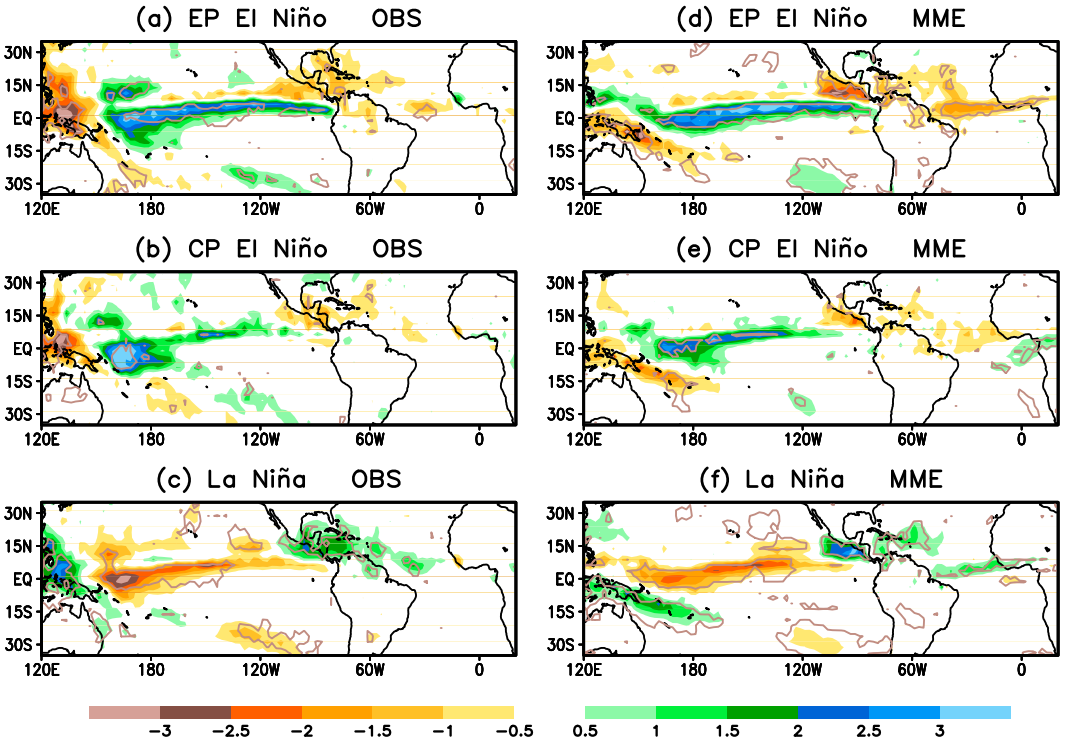

FIG. 10. Composites of ASO seasonal mean precipitation anomalies (mm day^{-1}) for (a),(d) EP El Niño; (b),(e) CP El Niño; and (c),(f) La Niña during 1982–2009 in (a)–(c) observations and (d)–(f) the MME mean. The anomalies circled by light gray lines are above the 99% significance level.

model bias in simulating the humidity variability. For example, the negative humidity anomalies to the north of the MDR during CP El Niño (Fig. 12d) coincide with the negative TC track density anomalies in the observations (Fig. 2e). In the MME mean, in contrast, the absence of these large TC track density anomalies and a less spatially coherent pattern in the same region (Fig. 6, bottom center) may be related to the weak variability of humidity associated with CP El Niño in the models (Fig. 12g).

Compared to EP El Niño (Fig. 2d), there are increased landfalling TCs over the southeastern United States associated with CP El Niño (Fig. 2e). However, the GCMs fail to capture this observed feature (Fig. 6, center). A recent study by Colbert and Soden (2012) demonstrated that the shift in TC tracks between El Niño

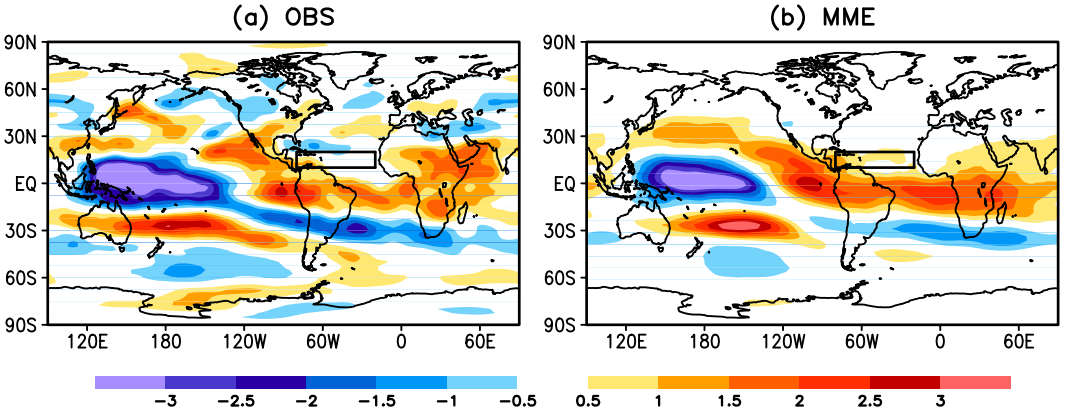

FIG. 11. Changes in vertical wind shear (m s^{-1} K^{-1}) associated with a westward shift of warm SST anomalies from the Niño-3 region (5°S–5°N, 90°–150°W) to the Niño-4 region (5°S–5°N, 150°W–160°E) for (a) observations and (b) the MME mean. The boxes with solid lines denote the MDR.

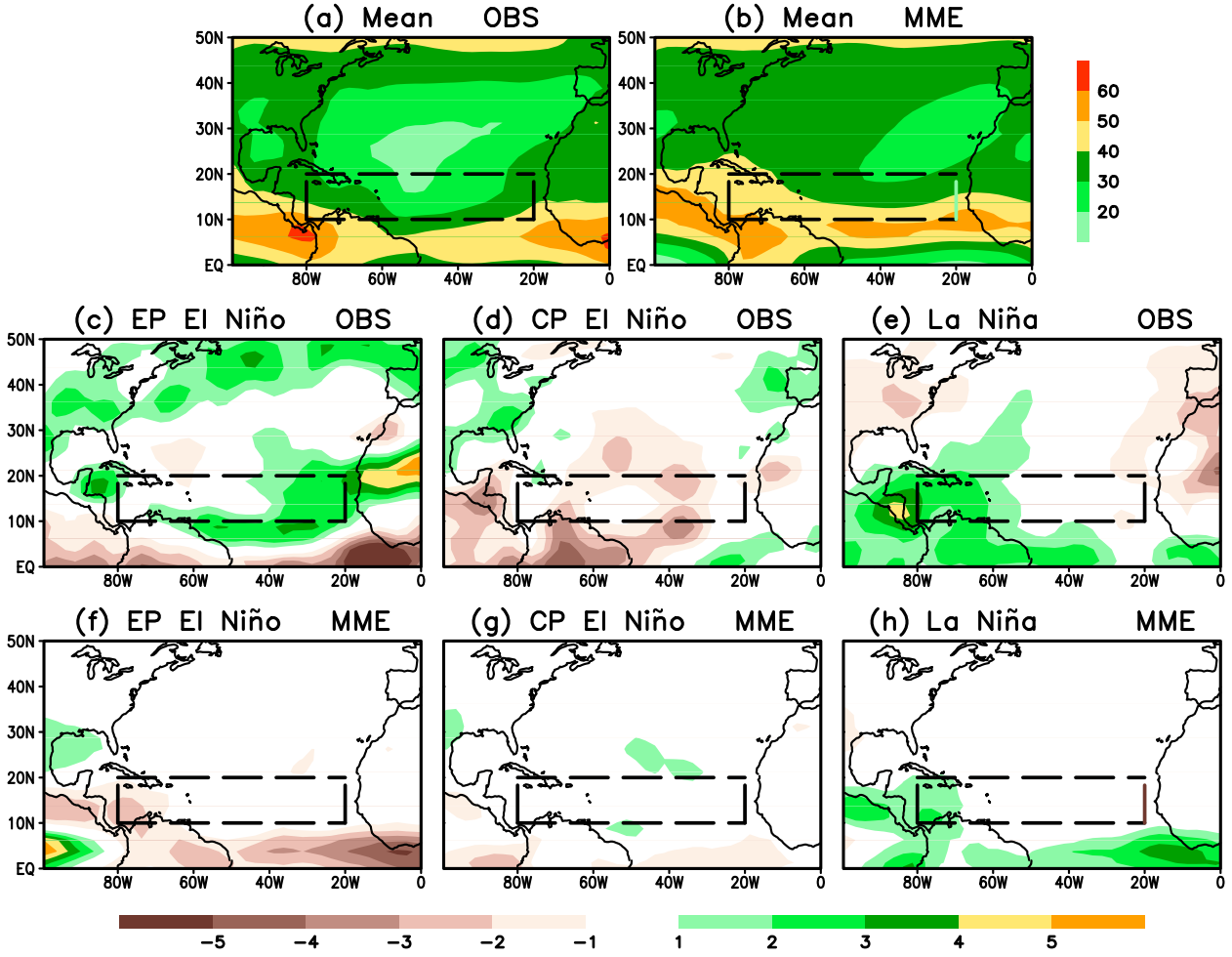

FIG. 12. ASO season climatology of 500-hPa relative humidity (%) in (a) observations and (b) the MME mean, and composites of ASO seasonal mean 500-hPa relative humidity anomalies (%) for (c),(f) EP El Niño; (d),(g) CP El Niño; and (e),(h) La Niña during 1982–2009 in (c)–(e) the observations and (f)–(h) the MME mean. The boxes with dashed lines denote the MDR.

and La Niña years is largely attributable to the variability of deep tropospheric steering flow. An analysis similar to Colbert and Soden (2012) is performed for the steering flow variations stratified not only by El Niño and La Niña events but also by EP and CP El Niño events. Figure 13 presents the composites of anomalous deep-layer steering flow in ASO associated with the three ENSO categories for both observations and the MME, respectively, superimposed onto the corresponding TC track density anomalies.

In the observations, the anomalous deep-layer steering flow is characterized by northwesterlies over the U.S. East Coast associated with EP El Niño (Fig. 13a) and easterlies over the Gulf of Mexico associated with La Niña (Fig. 13c). Consequently, there are less landfalling TCs along the East Coast in the EP El Niño years and higher TC track density over the Gulf in the La Niña years. Although the steering flows are weak in the MME mean, they display the same characteristics as the observations for EP El Niño and La Niña with consistent track density distributions (Figs. 13d,f). For CP El Niño, the increase in landfalling TCs over the southeastern Unites States is closely related to the enhanced southwesterly steering flow over this region. In contrast, the modeled TC steering flow over the same region is opposite to the observations, leading to near-normal TC tracks over the Southeast (Fig. 13e).

6. Summary and conclusions

Based on the analysis of the HWG interannual experiments, the GCM's performance in simulating the variability of Atlantic TCs associated with ENSO are assessed. The results indicate that each model has different mean biases in terms of track density and TC origin. Among the five models, the GFDL model with

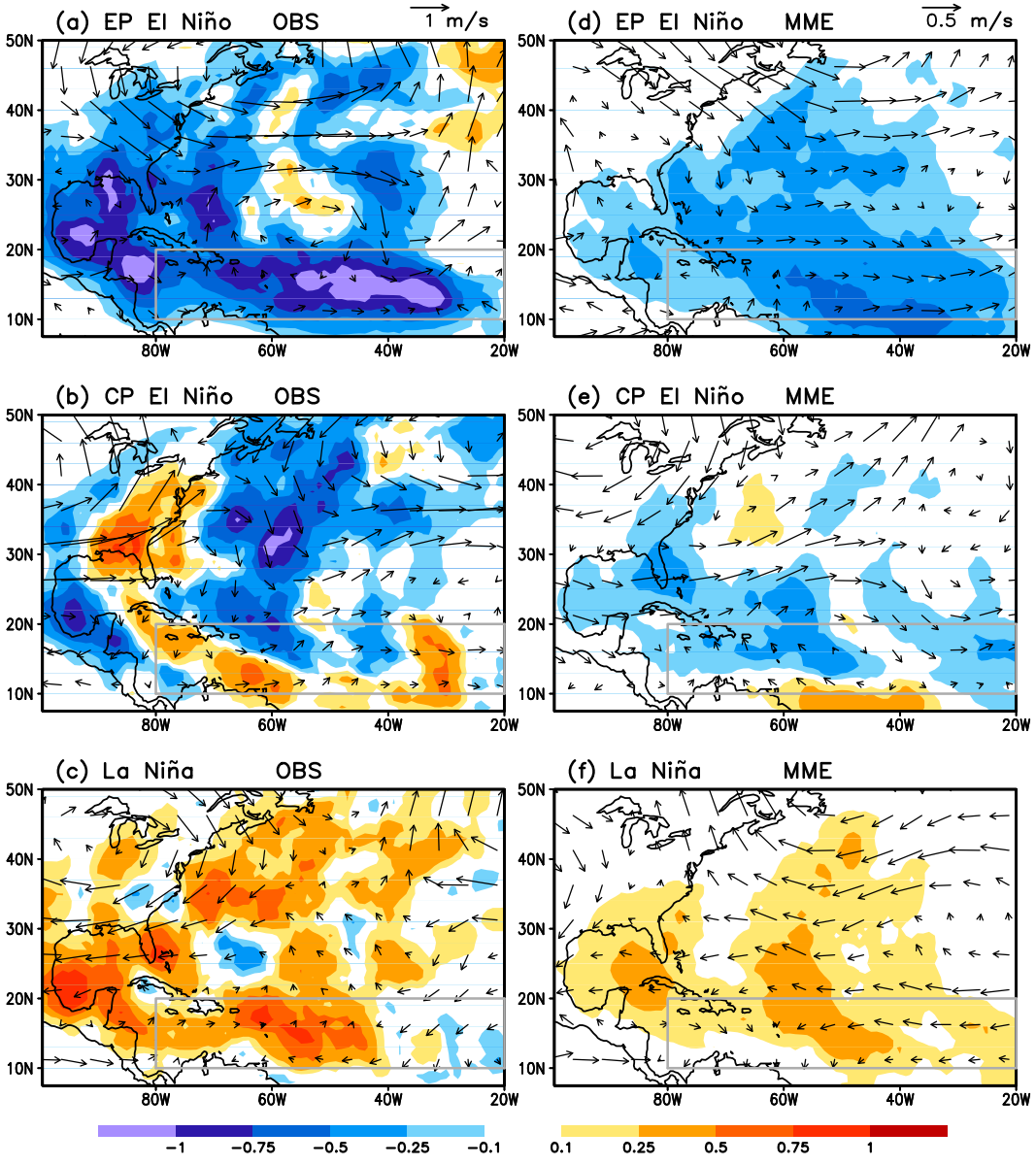

FIG. 13. Composites of ASO seasonal mean deep-layer steering flow anomaly (vectors; m s^{-1}) and TC track density anomaly (shadings) for (a),(d) EP El Niño; (b),(e) CP El Niño; and (c),(f) La Niña during 1982–2009 in (a)–(c) observations and (d)–(f) the MME mean. Arrow scales are given at the top of the left and right panels for the observations and MME, respectively. The boxes with gray lines denote the MDR.

a relatively high resolution has the best performance. The MME mean has the highest anomaly correlation for the number of TCs and the least RMSE. Therefore, using an MME should be considered a better approach for dynamical hurricane season prediction than using a single model, assuming that coupled GCMs can accurately predict global SST.

Overall, the GCMs simulate the variability of Atlantic TCs well with weaker activities during EP El Niño and stronger activities during La Niña. For CP El Niño, there is a slight increase in the number of TCs as compared with EP El Niño. However, the spatial distribution of track density and TC origin is less consistent among the models. Particularly, there is no indication of increasing TC activity over the U.S. southeast coastal region as found in observations. The differences between the models and the observations may be due to the bias of vertical wind shear in response to the shift of tropical heating associated with CP El Niño, as well as the model bias in the mean circulation. The models also have biases

in simulating the ENSO-related variations of the large-scale humidity field and deep-layer steering flow, both of which affect the genesis of TCs and the distribution of TC tracks. It should also be noted that there are limited sample sizes for both EP and CP El Niño events in the observations. The differences between EP and CP El Niño composites may not be just due to ENSO response, but may also contain some intersample variability.

There are at least two factors that may affect the results presented in this paper. One is the model sensitivity to different SST datasets (e.g., LaRow 2013). For example, the FSU model forced with the NOAA optimum interpolation SST, version 2 (OISST v2; Reynolds et al. 2002), may improve the simulations of Atlantic TC activity with a better TC climatology (11.5) and RMSE (4.5) than those forced with HadISST (Tables 2 and 3). Knowledge of the model sensitivity to SST forcing may help estimate the uncertainty of the model simulated TCs. In this study, different TC tracking algorithms were employed by the five modeling groups for their GCMs (Table 1). Track density and TC origin in the models may also be sensitive to the algorithms used. A unified tracking algorithm may be helpful to reduce the related uncertainty for model assessment. The sensitivity of TCs to tracking methods has been tested by the HWG with four GCMs, including the GISS and GFS models (M. Horn et al. 2014, unpublished manuscript). The analysis consists of a series of multimodel intercomparisons with TCs in different models but with a uniform TC detection method, as well as TCs in the same model but with different detection methods. The results are also reported in this special collection for the *Journal of Climate* (M. Horn et al. 2014, unpublished manuscript).

The impact of ENSO on Atlantic TC activity may have some implications for projections of future TC variability under a warming climate. Studies have shown an increase in tropical Atlantic wind shear (Vecchi and Soden 2007) and a reduction of Atlantic TCs associated with global warming with a high-resolution GCM (Zhao and Held 2010). In more recent studies, no robust changes in North Atlantic TC activity were found in the twenty-first-century simulations with low-resolution models (Camargo 2013; Tory et al. 2013). On the other hand, downscaling studies of these simulations lead to contradictory results, varying from a significant decrease (Knutson et al. 2013), ambiguous trends (Villarini and Vecchi 2012), to a significant increase (Emanuel 2013) in North Atlantic TC activity by the end of the twenty-first century. In addition to possible changes in the mean TC activity, the variability of TC activity is also expected to change as the intensity of CP El Niño (EP El Niño) would increase (decrease) under a warming climate (Kim and Yu 2012). In fact, CP El Niño has been documented to occur more frequently in the most recent two decades (Yeh et al. 2009), which could be a manifestation of global warming in observations.

There is a possibility that the relationship between Atlantic TC activity and ENSO under the present-day climate found in Kim et al. (2009) might not be maintained under a warming climate. Indeed, changes in atmospheric teleconnection in response to ENSO have been detected in model simulations for the twenty-first century (e.g., Stevenson 2012). This would add additional uncertainty to the future projection of Atlantic TC variability. Nevertheless, this study indicates the feasibility of utilizing high-resolution GCMs to assess the Atlantic TC activity associated with ENSO for climate change projections.

Acknowledgments. This work was carried out as part of a Hurricane Working Group activity supported by the U.S. CLIVAR. The authors thank the Lamont-Doherty Earth Observatory of Columbia University for archiving model data and making them accessible online. The authors also thank Prof. Kerry A. Emanuel, Dr. Christopher W. Landsea, Mr. Bill Mohan, an anonymous reviewer, and the editor for their insightful and constructive comments and suggestions.

REFERENCES

Ashok, K., S. K. Behera, S. A. Rao, H. Weng, and T. Yamagata, 2007: El Niño Modoki and its possible teleconnection. *J. Geophys. Res.,* **112,** C11007, doi:10.1029/2006JC003798.

Bell, G. D., and M. Chelliah, 2006: Leading tropical modes associated with interannual and multidecadal fluctuations in North Atlantic hurricane activity. *J. Climate,* **19,** 590–612, doi:10.1175/JCLI3659.1.

Camargo, S. J., 2013: Global and regional aspects of tropical cyclone activity in the CMIP5 models. *J. Climate,* **26,** 9880–9902, doi:10.1175/JCLI-D-12-00549.1.

——, and S. E. Zebiak, 2002: Improving the detection and tracking of tropical cyclones in atmospheric general circulation models. *Wea. Forecasting,* **17,** 1152–1162, doi:10.1175/1520-0434(2002)017<1152:ITDATO>2.0.CO;2.

——, A. G. Barnston, and S. E. Zebiak, 2005: A statistical assessment of tropical cyclone activity in atmospheric general circulation models. *Tellus,* **57A,** 589–604, doi:10.1111/j.1600-0870.2005.00117.x.

——, K. A. Emanuel, and A. H. Sobel, 2007: Use of a genesis potential index to diagnose ENSO effects on tropical cyclone genesis. *J. Climate,* **20,** 4819–4834, doi:10.1175/JCLI4282.1.

Cocke, S., and T. E. LaRow, 2000: Seasonal predictions using a regional spectral model embedded within a coupled ocean–atmospheric model. *Mon. Wea. Rev.,* **128,** 689–708, doi:10.1175/1520-0493(2000)128<0689:SPUARS>2.0.CO;2.

Colbert, A. J., and B. J. Soden, 2012: Climatological variations in North Atlantic tropical cyclone tracks. *J. Climate,* **25,** 657–673, doi:10.1175/JCLI-D-11-00034.1.

Emanuel, K. A., 2013: Downscaling CMIP5 climate models shows increased tropical cyclone activity over the 21st century. *Proc.*

Natl. Acad. Sci. USA, **110,** 12 219–12 224, doi:10.1073/pnas.1301293110.

Enfield, D. B., and D. A. Mayer, 1997: Tropical Atlantic sea surface temperature variability and its relation to El Niño–Southern Oscillation. *J. Geophys. Res.,* **102,** 929–945, doi:10.1029/96JC03296.

Fitzpatrick, P. J., J. A. Knaff, C. W. Landsea, and S. V. Finley, 1995: Documentation of a systematic bias in the aviation model's forecast of the Atlantic tropical upper-tropospheric trough: Implications for tropical cyclone forecasting. *Wea. Forecasting,* **10,** 433–446, doi:10.1175/1520-0434(1995)010<0433:DOASBI>2.0.CO;2.

Goldenberg, S. B., and L. J. Shapiro, 1996: Physical mechanisms for the association of El Niño and West African rainfall with Atlantic major hurricane activity. *J. Climate,* **9,** 1169–1187, doi:10.1175/1520-0442(1996)009<1169:PMFTAO>2.0.CO;2.

——, C. W. Landsea, A. M. Mestas-Nuñez, and W. M. Gray, 2001: The recent increase in Atlantic hurricane activity: Causes and implications. *Science,* **293,** 474–479, doi:10.1126/science.1060040.

Gray, W. M., 1984: Atlantic seasonal hurricane frequency. Part I: El Niño and 30 mb quasi-biennial oscillation influences. *Mon. Wea. Rev.,* **112,** 1649–1668, doi:10.1175/1520-0493(1984)112<1649:ASHFPI>2.0.CO;2.

Kanamitsu, M., W. Ebisuzaki, J. Woollen, S.-K. Yang, J. J. Hnilo, M. Fiorino, and G. L. Potter, 2002: NCEP–DOE AMIP-II Reanalysis (R-2). *Bull. Amer. Meteor. Soc.,* **83,** 1631–1643, doi:10.1175/BAMS-83-11-1631.

Kim, H.-M., P. J. Webster, and J. A. Curry, 2009: Impact of shifting patterns of Pacific Ocean warming on North Atlantic tropical cyclones. *Science,* **325,** 77–80, doi:10.1126/science.1174062.

Kim, S. T., and J.-Y. Yu, 2012: The two types of ENSO in CMIP5 models. *Geophys. Res. Lett.,* **39,** L11704, doi:10.1029/2012GL052006.

Knutson, T. R., and Coauthors, 2013: Dynamical downscaling projections of twenty-first-century Atlantic hurricane activity: CMIP3 and CMIP5 model-based scenarios. *J. Climate,* **26,** 6591–6617, doi:10.1175/JCLI-D-12-00539.1.

Kossin, J. P., S. J. Camargo, and M. Sitkowski, 2010: Climate modulation of North Atlantic hurricane tracks. *J. Climate,* **23,** 3057–3076, doi:10.1175/2010JCLI3497.1.

Kumar, A., and M. P. Hoerling, 1995: Prospects and limitations of seasonal atmospheric GCM predictions. *Bull. Amer. Meteor. Soc.,* **76,** 335–345, doi:10.1175/1520-0477(1995)076<0335:PALOSA>2.0.CO;2.

Landsea, C. W., 2000: El Niño/Southern Oscillation and the seasonal predictability of tropical cyclones. *El Niño and the Southern Oscillation: Multiscale Variability and Global and Regional Impacts,* H. F. Diaz and V. Markgraf, Eds., Cambridge University Press, 149–182.

——, and J. L. Franklin, 2013: Atlantic hurricane database uncertainty and presentation of a new database format. *Mon. Wea. Rev.,* **141,** 3576–3592, doi:10.1175/MWR-D-12-00254.1.

——, G. A. Vecchi, L. Bengtsson, and T. R. Knutson, 2010: Impact of duration thresholds on Atlantic tropical cyclone counts. *J. Climate,* **23,** 2508–2519, doi:10.1175/2009JCLI3034.1.

LaRow, T. E., 2013: The impact of SST bias correction on North Atlantic hurricane retrospective forecasts. *Mon. Wea. Rev.,* **141,** 490–498, doi:10.1175/MWR-D-12-00152.1.

——, Y.-K. Lim, D. W. Shin, E. P. Chassignet, and S. Cocke, 2008: Atlantic basin seasonal hurricane simulations. *J. Climate,* **21,** 3191–3206, doi:10.1175/2007JCLI2036.1.

McPhaden, M. J., T. Lee, and D. McClurg, 2011: El Niño and its relationship to changing background conditions in the tropical Pacific Ocean. *Geophys. Res. Lett.,* **38,** L15709, doi:10.1029/2011GL048275.

Molod, A., L. Takacs, M. Suarez, J. Bacmeister, I.-S. Song, and A. Eichmann, 2012: The GEOS-5 Atmospheric General Circulation Model: Mean climate and development from MERRA to Fortuna. NASA Tech. Rep. NASA/TM-2012-104606, Vol. 28, 117 pp. [Available online at http://gmao.gsfc.nasa.gov/pubs/docs/tm28.pdf.]

NOAA, cited 2013: Atlantic hurricane outlook and summary archive. [Available online at http://www.cpc.ncep.noaa.gov/products/outlooks/hurricane-archive.shtml.]

Peng, M. S., B. Fu, T. Li, and D. E. Stevens 2012: Developing versus nondeveloping disturbances for tropical cyclone formation. Part I: North Atlantic. *Mon. Wea. Rev.,* **140,** 1047–1066, doi:10.1175/2011MWR3617.1.

Pielke, R. A., Jr., and C. W. Landsea, 1999: La Niña, El Niño, and Atlantic hurricane damages in the United States. *Bull. Amer. Meteor. Soc.,* **80,** 2027–2033, doi:10.1175/1520-0477(1999)080<2027:LNAENO>2.0.CO;2.

Rayner, N. A., D. E. Parker, E. B. Horton, C. K. Folland, L. V. Alexander, D. P. Rowell, E. C. Kent, and A. Kaplan, 2003: Global analyses of sea surface temperature, sea ice, and night marine air temperature since the late nineteenth century. *J. Geophys. Res.,* **108,** 4407, doi:10.1029/2002JD002670.

Reynolds, R. W., N. A. Rayner, T. M. Smith, D. C. Stokes, and W. Wang, 2002: An improved in situ and satellite SST analysis for climate. *J. Climate,* **15,** 1609–1625, doi:10.1175/1520-0442(2002)015<1609:AIISAS>2.0.CO;2.

Rienecker, M. M., and Coauthors, 2008: The GEOS-5 Data Assimilation System—Documentation of versions 5.0.1 and 5.1.0, and 5.2.0. NASA Tech. Rep. NASA/TM-2008-104606, Vol. 27, 92 pp. [Available online at http://gmao.gsfc.nasa.gov/pubs/docs/Rienecker369.pdf.]

Saha, S., and Coauthors, 2014: The NCEP Climate Forecast System version 2. *J. Climate,* **27,** 2158–2208, doi:10.1175/JCLI-D-12-00823.1.

Sardeshmukh, P. D., and B. J. Hoskins, 1988: The generation of global rotational flow by steady idealized tropical divergence. *J. Atmos. Sci.,* **45,** 1228–1251, doi:10.1175/1520-0469(1988)045<1228:TGOGRF>2.0.CO;2.

Schemm, J.-K. E., and L. Long, 2009: Dynamic hurricane season prediction experiment with the NCEP CFS CGCM. *Extended Abstracts, NOAA CTB Joint Seminar Series,* Calverton, MD, IGES/COLA, NOAA, Vol. 3, 27–29. [Available online at http://www.nws.noaa.gov/ost/climate/STIP/FY09CTBSeminars/CollectionVol_FY09CTBJS.pdf.]

Schmidt, G. A., and Coauthors, 2014: Configuration and assessment of GISS ModelE2 contributions to the CMIP5 archive. *J. Adv. Model. Earth Syst.,* **6,** 141–184, doi:10.1002/2013MS000265.

Stevenson, S. L., 2012: Significant changes to ENSO strength and impacts in the twenty-first century: Results from CMIP5. *Geophys. Res. Lett.,* **39,** L17703, doi:10.1029/2012GL052759.

Tang, B. H., and J. D. Neelin, 2004: ENSO influence on Atlantic hurricanes via tropospheric warming. *Geophys. Res. Lett.,* **31,** L24204, doi:10.1029/2004GL021072.

Tory, K. J., S. S. Chand, J. L. McBride, H. Ye, and R. A. Dare, 2013: Projected changes in late-twenty-first-century tropical cyclone frequency in 13 coupled climate models from phase 5 of the Coupled Model Intercomparison Project. *J. Climate,* **26,** 9946–9959, doi:10.1175/JCLI-D-13-00010.1.

U.S. CLIVAR, 2011: U.S. CLIVAR launches two new working groups. *U.S. Clivar Variations,* Vol. 9, No. 1, U.S. CLIVAR

Office, Washington, DC, 12 pp. [Available online at http://www.usclivar.org/sites/default/files/Variations-V9N1-1.pdf.]

Vecchi, G. A., and B. J. Soden, 2007: Increased tropical Atlantic wind shear in model projections of global warming. *Geophys. Res. Lett.,* **34,** L08702, doi:10.1029/2006GL028905.

——, M. Zhao, H. Wang, G. Villarini, A. Rosati, A. Kumar, I. M. Held, and R. Gudgel, 2011: Statistical–dynamical predictions of seasonal North Atlantic hurricane activity. *Mon. Wea. Rev.,* **139,** 1070–1082, doi:10.1175/2010MWR3499.1.

Villarini, G., and G. A. Vecchi, 2012: Twenty-first-century projections of North Atlantic tropical storms from CMIP5 models. *Nat. Climate Change,* **2,** 604–607, doi:10.1038/nclimate1530.

——, ——, T. R. Knutson, and J. A. Smith, 2011: Is the recorded increase in short-duration North Atlantic tropical storms spurious? *J. Geophys. Res.,* **116,** D10114, doi:10.1029/2010JD015493.

Wang, H., J.-K. E. Schemm, A. Kumar, W. Wang, L. Long, M. Chelliah, G. D. Bell, and P. Peng, 2009: A statistical forecast model for Atlantic seasonal hurricane activity based on the NCEP dynamical seasonal forecast. *J. Climate,* **22,** 4481–4500, doi:10.1175/2009JCLI2753.1.

——, A. Kumar, W. Wang, and B. Jha, 2012: U.S. summer precipitation and temperature patterns following the peak phase of El Niño. *J. Climate,* **25,** 7204–7215, doi:10.1175/JCLI-D-11-00660.1.

——, Y. Pan, A. Kumar, and W. Wang, 2013: Modulation of convectively coupled Kelvin wave activity in the tropical Pacific by ENSO. *Acta Meteor. Sin.,* **27,** 295–307, doi:10.1007/s13351-013-0306-5.

Wilks, D. S., 1995: *Statistical Methods in the Atmospheric Sciences: An Introduction.* Academic Press, 467 pp.

Xie, P., and P. A. Arkin, 1997: Global precipitation: A 17-year monthly analysis based on gauge observations, satellite estimates, and numerical model outputs. *Bull. Amer. Meteor. Soc.,* **78,** 2539–2558, doi:10.1175/1520-0477(1997)078<2539:GPAYMA>2.0.CO;2.

Yeh, S.-W., J.-S. Kug, B. Dewitte, M.-H. Kwon, B. P. Kirtman, and F.-F. Jin, 2009: El Niño in a changing climate. *Nature,* **461,** 511–514, doi:10.1038/nature08316.

Zhao, M., and I. M. Held, 2010: An analysis of the effect of global warming on the intensity of Atlantic hurricanes using a GCM with statistical refinement. *J. Climate,* **23,** 6382–6393, doi:10.1175/2010JCLI3837.1.

——, ——, S.-J. Lin, and G. A. Vecchi, 2009: Simulations of global hurricane climatology, interannual variability, and response to global warming using a 50-km resolution GCM. *J. Climate,* **22,** 6653–6678, doi:10.1175/2009JCLI3049.1.